A MESOSCALE MODELLING PERSPECTIVE OF CRACKING PROCESS AND FRACTURE ENERGY UNDER HIGH STRAIN RATE TENSION

Y. LU [*], J. XU [*] AND J. WEERHEIJM [†]

[*] University of Edinburgh
Institute for Infrastructure and Environment, School of Engineering, Edinburgh EH9 3JL, UK
e-mail: yong.lu@ed.ac.uk, www.see.ed.ac.uk

[†] Delft University of Technology
Faculty of Civil Engineering and Geosciences, Delft, The Netherlands
& TNO, Defence Safety and Security, Rijswijk, The Netherlands
e-mail: J.Weerheijm@tudelft.nl, www.tudelft.nl/; www.tno.nl

Key words: concrete, dynamic tension, high strain rate, fracture energy, mesoscale model

Abstract: This paper presents a numerical modelling study on the simulation of the cracking process and fracture energy in concrete under high strain rate. To capture the stress wave effect and the damage evolution at the meso-length scale, both a homogeneous model with a millimetre-resolution mesh and an explicit heterogeneous mesoscale model with random polygon aggregates are employed. The tendency of development of a) discrete multiple cracks, and b) spread tensile damage across adjacent element layers, in the high strain rate tension regime is scrutinised. This phenomenon generally gives rise to an increase in the dynamic fracture energy, which is consistent with experimental observations. Relative comparison between the homogeneous and heterogeneous mesoscale simulations suggests a sensible effect of the mesoscopic heterogeneity in the dynamic fracture process.

1 INTRODUCTION

The dynamic behaviour of concrete has been a subject of continuous research interest over the last few decades. A major focus has been identification of the mechanisms underlying the apparent increase of the dynamic strength or the so-called DIF, both in compression and tension, under high strain rate loading. It has been generally recognised that, while the DIF in compression has much to do with the macroscopic dynamic structural effect (in particular the inertia confinement) (e.g. [1-4]), the increase in the dynamic tensile strength is not significantly affected by such a macroscopic dynamic mechanism, and may therefore only be attributed to local effects at the micro-meso scale levels ([5-7]), along with

a varying degree of influence by the free water content. Therefore, unless an appropriate representation of the above mentioned micro-physical mechanisms is incorporated in the computational model, the increase in the dynamic tensile strength would have to be treated as a property in the material model.

This paper is concerned about another important aspect of the dynamic material characterisation, namely the dynamic fracture process and the absorbed energy represented by the parameter G_f, the fracture energy. In the computational model the G_f value affects the distribution of cracks and the overall softening behaviour. Fracture energy under quasi-static tension loading is generally well understood and empirical formulas exist for the calculation of fracture energy for a given grade

and composition of concrete (e.g. [8]). Experimental evidences suggest that fracture energy tends to increase with the tensile strain rate. However, only a limited amount of experimental data on dynamic fracture energy is available. Weerheijm [9] measured the fracture energy by SHB direct tension test at rates between 10^{-1} and 10^{0} s^{-1} and observed no sensible increase of fracture energy in this rate range. Schuler et. al. [10], Weerheijm and Doormaal [11] and Vegt and Weerheijm [16] conducted dynamic spalling tests for plain concrete in the strain rates between 20 and 100 s^{-1}, and a steep increase in the fracture energy at these strain rates was measured in these experiments. Experiment carried out by Brara and Klepaczko [12] also suggested a drastic increase of fracture energy in the loading rate around 1000 GPa/s.

In the present study, we undertake to simulate the dynamic fracture process and fracture energy in concrete under high strain rate tension using a damage-based continuum model and the dynamic analysis code LS-DYNA. To capture the stress wave effect and the damage evolution at the meso-length scale, both a homogeneous model with however a millimetre-resolution mesh and a heterogeneous mesoscale model are employed. Fracture is modelled in a smeared manner as is typically exercised in FE modelling of concrete, along with a mesh-objective constitutive material model which is aimed to enable a mesh-independent (global) softening behaviour and preservation of specific fracture energy. Such a scheme is proven to work out satisfactorily under quasi-static and relatively low strain rate tension. One of the objectives of this study is to test the performance of such a modelling approach when it is applied for high strain rate tension simulations. The tendency of development of a) discrete multiple cracks, and b) spread fracture across adjacent element layers, in the high strain rate tension regime will be examined. Such a phenomenon generally gives rise to an increase in the dynamic fracture energy, which is consistent with experimental observations. Relative comparison between the homogeneous and heterogeneous mesoscale

simulations suggests a sensible contribution of the mesoscopic heterogeneity in distributing the tensile damage and affecting the fracture energy. It should be noted that as the stress, strain and in particular strain rate field becomes more complicated, numerical treatments such as the mesh-objective softening regularisation in a smeared crack context will need to be examined thoroughly in terms of their representativeness of the local processes in light of the highly transient stress wave effect. This will be discussed in a subsequent study.

2 EXPERIMENTAL BACKGROUND

Many experiments have been performed to determine the tensile strength at varied strain rates (loading rates), whereas only a few of them involve measurement of fracture energy. Three types of Hopkinson Bar based dynamic tensile tests are suitable for this study, namely direct tension test, dynamic splitting test and spalling test, depending upon the strain rate ranges of interest. Among these methods, spalling test can achieve strain rate higher than 10 s^{-1} and up to 100 s^{-1}. Details about a spalling test setup can be found in [11, 16]. Table 1 gives a list of a few spalling tests conducted in recent years.

Table 1: Summary of selected spalling tests (length unit: mm)

Ref.	Strain rate	DIF of tensile strength	Loading	Specimen length	Dia.
[11]	20.0~25.5	4.83~8.5	detonator	240	74
[10]	23.5~93.6	4.1~6.8	projectile	250	74.2
[13]	20~120	3~12	projectile	120	40
[16]	~40	~3#	detonator	300	74

notched specimen

In determining the dynamic Young's modulus, the first step is to re-construct (by shifting) the compressive wave acting on the specimen through the incident bar-specimen interface. The following governing equations may be used to deduce the dynamic modulus.

$$C_0 = \frac{L}{\Delta t} \qquad (1)$$

$$E_{dy} = \rho C_0^2 \qquad (2)$$

where C_0 is the wave speed, Δt is the time interval that the wave needs to propagate from the beginning to the end of the specimen.

The tests in [11] gave a dynamic modulus increase factor of 1.25, whereas no significant increase in the dynamic modulus was reported in [10]. On the other hand, CEB [8] provides a formula for the calculation of the dynamic Young's Modulus of concrete under compression. For strain rates ranging between 20 and 100 s^{-1}, this formula yields an increase factor of 1.42~1.48. Comparing to the experimental data considered herein, the CEB formula appears to over-predict the dynamic Young's modulus. It should be noted that because of adoption of a linear elastic assumption, the Young's modulus value will have a significant influence on the calculated strain rate as well as the spall strength if strain gauges are to be used to deduce the dynamic strength.

Several techniques have been proposed to evaluate the dynamic tensile strength of concrete in a spalling test, using respectively a strain-based and a velocity-based measurement setup. The method introduced by Weerheijm and Van Doormaal [11] is based on strain measurements in the concrete specimen, as shown in Fig. 1. According to elastic wave analysis the first fracture plane in this particular specimen lies at about 70mm from the free end, which is between strain gauge S6 and S7. The transmitted compressive pulse from incident bar is given by the mean value of S1~S4. A basic assumption is that the concrete remains linear-elastic and experience no ductility. Thus location S5, which is deemed to be beyond the tensile fracture zone and not to fail, is taken as a reference to deduce the stress that passes through the fracture line, by multiplying the recorded strain by the dynamic Young's modulus. Note that this technique was improved by Vegt et al. [16] and combined with direct deformation

measurements for the fracture zone on notched specimen. In the current paper we shall confine ourselves on specimens without a notch, which are more commonly reported in literature. Thus only the results of the un-notched specimen in [11] are used as a reference in the current paper.
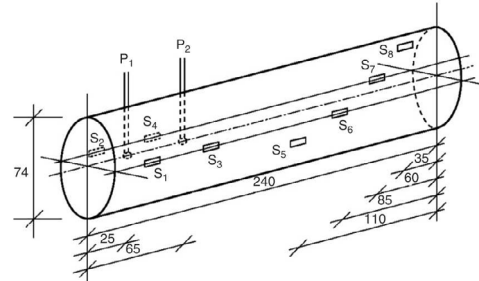

Figure 1: Instrumentation of concrete specimen [11].

Another way to deduce the dynamic tensile strength was initially derived from spalling tests performed on metals by the plate-impact technique. This approach adopts a linear acoustic approximation to obtain the spall strength from the pull-back velocity recorded at the rear face of the specimen:

$$\sigma_{dyt} = \frac{1}{2}\rho C_0 \Delta V_{pull-back} \qquad (3)$$

The pull-back velocity is defined as the difference in the free end velocity between the maximum and the velocity at rebound. The underlying assumption is that the material behaves linear elastically in-between the cracking plane, which initiates the rebound, and the rear face. The same method has been used in the study by Schuler et al. [10].

As for the measurement of the dynamic fracture energy, unlike quasi-static test, there is no direct way to measure the development of crack opening and unloading of the specimen under high loading rate, except for a notched specimen [16, 17]. For an un-notched specimen, mainly two techniques have been proposed to evaluate the fracture energy of concrete. The first method, as presented by Weerheijm and Van Doormaal [11], is based on the energy balance among the compression pulse, the energy trapped in the spall debris, and the tensile pulse beyond the failure zone and the fracture energy. Assuming only one

fracture zone occurs and the concrete specimen is linear-elastic except in the fracture zone, all energy dissipated in the fracture zone is due to the fracture energy, thus:

$$E_{compr} = E_{debr} + E_{trans,tens} + E_{frac} \qquad (4)$$

The energy of the compressive and the transmitted tensile pulse, E_{compr} and $E_{trans,tens}$, can be determined by the strain recordings along the specimen length. The kinetic energy term E_{debr} can be obtained from the measured velocity history of the spalling debris. The fracture energy G_f is then determined by E_{frac} divided by the cross-sectional area.

The second method was reported in Schuler et al. [10]. The fracture energy is regarded as the integral of the force over the crack opening and can be written as a function of the impulse change and the crack opening velocity. Over the whole fracture process the impulse transferred from one fragment to the next can be determined, and this is then used in the calculation of the fracture energy.

3 NUMERICAL MODEL AND BASIC ASSUMPTIONS

3.1 General model set-up

Herein we consider the specimens tested by Weerheijm and Van Doormaal [11] for the numerical investigation. The experimental data suggests a dynamic fracture energy increase factor of around 2~3 for a strain rate in the range of 20~100 s^{-1}. This numerical simulation study is aimed to explore the possible mechanisms, particularly in terms of the dynamic fracture development from a mesoscopic point of view. We first simulate the experiment using a homogeneous finite element model with however a mesh resolution sufficiently fine to expose the dynamic process at a meso-length scale. This will be complemented by an examination of the possible contribution of the mesoscopic heterogeneity, which will come later in Section 5.

The cylindrical specimens have an overall dimension of 240mm in length and 74mm in diameter. The concrete material tested has a density 2350 kg/m^3, and static properties of Young's modulus 37 GPa, compressive strength 40 MPa, tensile strength 3 MPa, Poisson's ratio 0.2. The (static) fracture energy (G_f) is assumed to be 65 N/m in the simulation considering a nominal aggregate size of 8 mm.
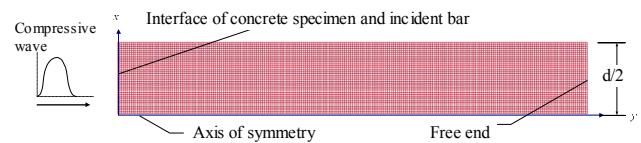

Figure 2: Axisymmetric FE model for spalling test.

In the finite element analysis, the specimen is modelled using a 2D axis-symmetrical model. Fig. 2 shows the overall model configuration and a typical mesh. The mesh resolution is around 1 mm.

3.2 Loading and boundary conditions

It is possible to include the entire SHB test set-up in the numerical simulation, but for the purpose of controlling the computational cost, herein we only model the test specimen with the loading being simulated by an appropriate compressive pressure history. Such a simplification is commonly adopted in the numerical simulation of this class of problems. For confirmation purpose a comparative simulation exercise was conducted, in which a test was simulated both by a model including the SHB bars and a simplified model with directly imposed load pulse. The results showed that the response of the concrete specimen as represented by the free end velocity were more or less identical for both models, given that the pressure pulse applied in the simplified model matches that at the actual specimen-incident bar interface. Fig. 3 shows a typical comparison of the specimen free end velocity histories using the two modelling schemes. For the simplified model the loading is applied via a pressure pulse or a velocity boundary at the loading face, and these turn out to produce effectively the same results.
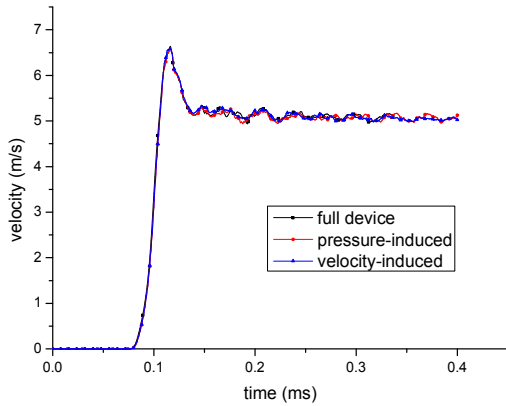
Figure 3: Free end velocity comparison.

The imposed compressive pressure history in the present numerical simulation is generated in accordance with the experimental data measured during the tests [11]. The duration of the loading pulse is in the order of 70 μs with a 50 μs rising and 20 μs descending branches. Fig. 4 gives a typical curve of a loading pulse of 25MPa. Different strain rates are achieved by scaling up or down the peak amplitude while keeping the duration.
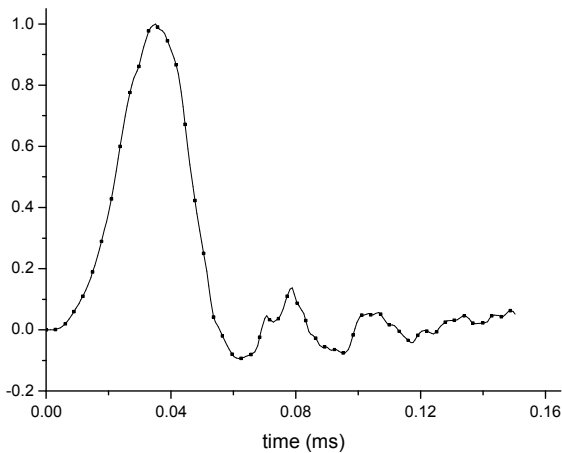

Figure 4: Typical pressure input as stress boundary.

3.3 Concrete material model and mesh-objective preservation of fracture energy (Gf)

The material model employed in this study is the CSCM (Continuous Surface Cap Model) (or Concrete Model 159 in LS-DYNA). In this model, the failure surfaces are defined by three invariants together with the cap hardening parameter. Parameters defining the failure

surfaces are determined by fitting triaxial tensile and compressive test data. Damage is applied by directly multiplying a scalar damage index to the stress tensor, after updated by the visco-plasticity algorithm, where rate effect is incorporated. Both strain softening and modulus degradation are considered. Details about the model formulation can be found in [14]. In what follows, two important aspects of the material model which require special attention in the present simulation are highlighted.

The first is about the consideration of damage evolution. In CSCM, brittle (tension) and ductile (compression) damage are separately recorded, such that brittle damage accumulation depends on the maximum principal strain whereas ductile damage accumulation depends on the total strain components. The damage index applied to the stress tensor is equal to the current maximum of the brittle or ductile damage index. In order to simulate the crack recovery, an externally input parameter is employed to control the recovery of compressive stiffness. With its default value, ductile damage never decreases, but brittle damage drops to zero, which means stiffness is fully recovered, whenever the pressure switches from tensile to compressive. Once the pressure enters tensile again, previous brittle damage value will be reactivated. This scheme allows for a rational realisation of the crack opening and closure cycles.

Another aspect is on the handling of strain softening. Like many other similar material models, the stress and strain relation in the tension softening branch is made dependent upon the mesh size, through a characteristic element length L_c, such that the total softening energy (per unit cross section) over L_c would remain constant and equal to the fracture energy:

$$\int_{\varepsilon_m}^{+\infty} \sigma d\varepsilon = \frac{G_f}{L_c} \qquad (5)$$

In this way, when damage localisation into a single element width (L_c) occurs, which would be inevitable in a tension-dominated

response in a local FE model, the target fracture energy is conserved regardless the mesh size, thus facilitating a relatively mesh independent (global) softening behaviour.

It should be noted that when the CSCM model is applied in a 2D axisymmetric model, the current algorithm as implemented in LS-DYNA treats the "thickness" of each element as the arc length over a unit radiant in the implied circumferential direction. It follows that elements of the same size on the 2D plane but at different distances from the axis of symmetry are evaluated to be of different volume and hence of different characteristic length, and consequently will have different softening branch in the stress-strain curve. This is not the expected outcome of the mesh-objective treatment of the stress-strain relationship for a 2D axisymmetric problem, in that the softening behaviour should only be dependent upon the element size on the 2D plane but not on the locations with respect to the axis of symmetry. In the present simulation this problem is addressed indirectly by modifying artificially the fracture energy input for different layers of elements with respect to the distance to the axis of symmetry such that the eventually achieved fracture energy will be equal to the targeted amount of fracture energy for the 2D characteristic length.

3.4 Tensile DIF and rate-independent "baseline" fracture energy

The dynamic increase of the tensile strength is primarily attributable to time-dependent micro-mechanical processes (see [17]) which are not represented in the current finite element model. Consequently it is only logical to incorporate an adequate tensile DIF at the material model level, i.e., as a material property, in the present simulation study. In this way the model is capable of realising a real time strain-rate dependent dynamic tensile strength during the course of the tension loading, allowing for an investigation of the effects of the dynamic processes at the meso- and global scales on the dynamic tension behaviour and the dynamic energy dissipation.

In CSCM the strain rate enhancement is

incorporated through a two-parameter formulation, so that separate compressive and tensile rate effects can be considered. The default tensile DIF curve is adopted here, which is similar to the modified CEB formula with a much increased DIF magnitude as compared to the standard CEB curve. Further investigation into the adequacy of a particular DIF formula in a meso-level modelling study and the implications on the interpretation of experimental tensile DIF data will be carried out in a subsequent study.

On the other hand, to avoid complications arising from arbitrary rate dependency of the fracture energy, herein we adopt the hypothesis that the fracture energy on a per-element basis (which is essentially per macro-crack in the context of the crack-band theory) is not dependent on the strain rate. As a result any increase in the achieved fracture energy in the dynamic simulation will be attributable to the meso- (local) and global scale dynamic effects, as will be elaborated later. Fig. 5 illustrates the tensile stress-strain curves as obtained from single element trials, from which the achieved effects of implementing DIF and rate-independent fracture energy on the tensile strength and the softening branch as the strain rate varies are clearly observable.
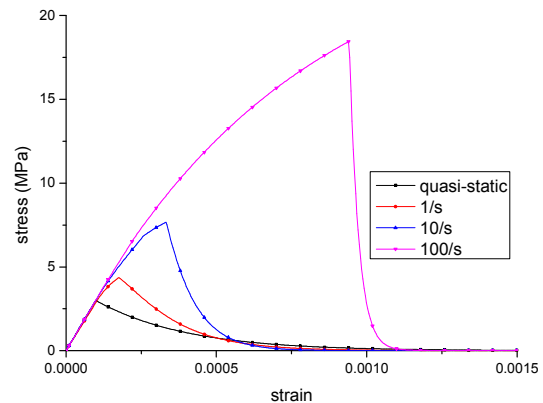

Figure 5: Tensile stress-strain curves generated by the material model

4 PRELIMINARY NUMERICAL SIMU-LATION STUDIES AND DISCUSSION

In what follows we shall present some preliminary numerical simulations of the spalling tests conducted by Weerheijm and Van Doormaal [11]. The loading rate in the

experiment was 920 GPa/s, with a target strain rate on an order of 20 s⁻¹.

As the material model does not consider strain rate effect on the Young's modulus, the Young's modulus in the simulation is purposely assigned to match the dynamic modulus obtained from the experiment, i.e., about 46 GPa, so as to ensure a wave propagation velocity during the dynamic loading to be consistent with the experiment. All other material parameters tally with the experimental data, except that the static fracture energy value, which was not specified in the original paper, is assigned 69.4 N/m according to CEB Model Code [8].

Fig. 6 illustrates the plastic strain and tensile damage contours for a pulse load similar to that achieved in the experiment. The macro crack plane occurs at about 68mm from the free end, which agrees well with the experimental result as well as the theoretical prediction. Despite a distinctive single macro crack from the plastic strain contour, the damage contour demonstrates an apparent tensile damage zone over a band width of about 30mm. This is in contrast to the scenario under a lower rate tension, where both the plastic strain and the damage are more or less concentrated in a single element layer. As a result of the spread of the tensile damage, the overall amount of energy dissipated within the fracture band increases, which transpires to an increased fracture energy on a per crack-band basis.
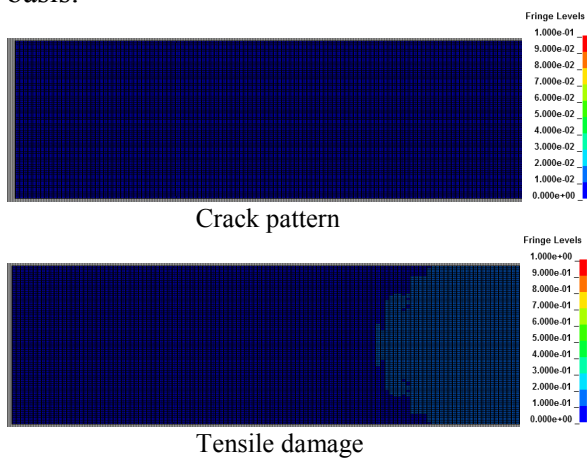

Crack pattern

Tensile damage

Figure 6: Simulated results of macro crack pattern (upper, represented by final plastic strain) and tensile damage (lower)
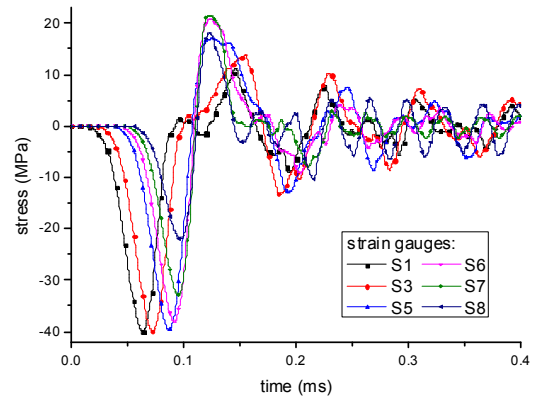

Figure 7: Simulated stress histories at different locations of specimen

Fig. 7 plots the stress histories at locations where the strains were measured during the experiment. Considering a certain strain gauge length, the stress values from the simulation results are obtained by averaging the stresses in elements within a 6-mm length centred at a particular position on the specimen surface. The location of the strain gauge plan has been given in Fig. 1. The peak tensile stress reaches about 20 MPa, which indicates the magnitude of the dynamic tensile strength achieved in the specimen.

Besides the above direct reading of the dynamic stress from the simulation, it is also instructive to examine the outcome of applying the alternative approach, i.e. using the pullback velocity at the free end to deduce the dynamic tensile strength, as given in Eq. 3. Fig. 8 shows the free end velocity history from the simulation. The dynamic tensile strength so obtained is about 27MPa, which is higher than the result directly obtained from the local elements (refer to Table 2). This discrepancy suggests that the approach based on the pull-back velocity at the free end could become unreliable for the present situation. Indeed this theory is based on the assumption that the rapture of specimen is instant and is associated with a sudden disruption to the wave propagation, whereas as observed clearly from the simulation a realistic spalling event would involve more or less a nonlinear softening process.
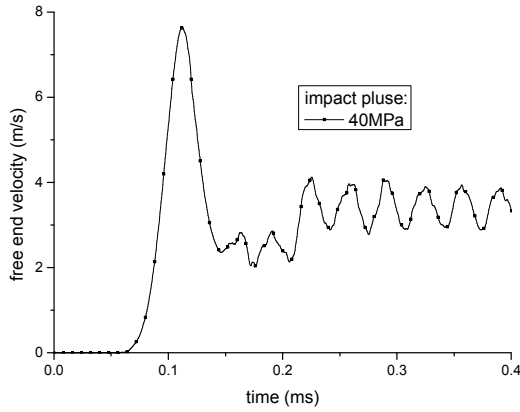
Figure 8: Free end velocity from the simulation

Table 2: Summary of experimental and numerical dynamic tensile strengths

	Strain-stress reading (MPa)	Spall strength (MPa)	Impact pulse (MPa)	Strain rate (1/s)	Load rate (GPa/s)
Exp.	18.4	/	/	20	920
FE	21.4	27.2	40	35	1620
Meso.	18.0	18.0	30	24	1114

To further examine the trend of the fracture damage spread under high strain rate tension, several additional tests are carried out with increased pulse pressure and therefore increased strain rate. Fig. 9 shows two examples of the tensile damage contours for peak loading of 60 MPa and 80 MPa, respectively.
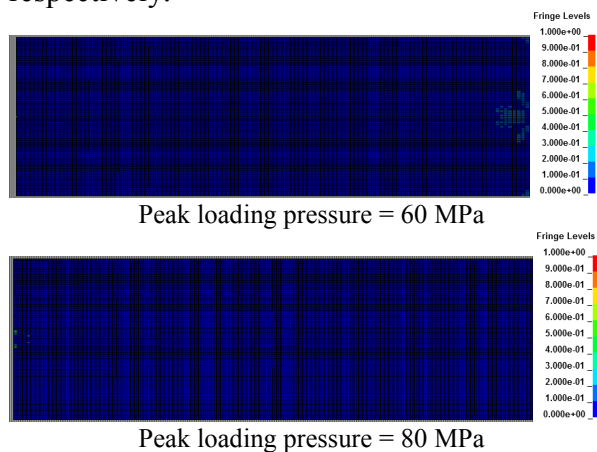

Peak loading pressure = 60 MPa

Peak loading pressure = 80 MPa

Figure 9: Damage values representing the fracture patterns under increased peak imposed pressure (and loading rate).

Table 3: Estimated fracture energy

	Pulse amplitude (MPa)	Strain rate (1/s)	Loading rate (GPa/s)	Total Gf (N/m)
Exp.[11]	27-30	20	920	310-340
FE model	40	35	1620	442
	60	59	2733	836
	80	76	3510	638
Meso	30	24	1114	193
	40	36	1666	337
	60	55	2532	573
	80	73	3395	1346

Comparing to the damage under peak loading of 40 MPa shown in Fig. 6, it can be seen that with the further increase of the loading magnitude and rate, discrete macro cracks start to appear within the extended tensile damage band, giving rise to a cluster of closely-spaced multiple cracks. This further increases the energy dissipated within the extended fracture zone, leading to a further increase in the overall dynamic fracture energy absorbed in the whole specimen. The general phenomenon is actually in a broad agreement with observations made in [10], where multiple macro cracks and ultimately fragmentation develops in the high rate spalling tests. A comparison of the dynamic fracture energy from the experiment and the numerical simulation is given in Table 3.

5 EXPLICIT MESOSCALE MODEL AND SIMULATION

A mesoscale model including explicit aggregates (random polygons) and the mortar matrix is generated to simulate the spall experiment. The mesoscale model is generated following the procedure described in [15], and the overall volume fraction of aggregates is set to be about 40%. The mesh resolution is similar to that used in the homogeneous FE model, with a nominal gird size of 1mm. ITZ is approximately represented by a layer of solid element surrounding each aggregate. Considering the weakening effect of the real ITZ, the equivalent ITZ layer is given a

reduced strength from the mortar matrix. In the present simulation for a standard concrete tensile strength of 3 MPa, the mortar elements are assigned a tensile strength of 3.5 MPa, whilst those of the equivalent ITZ are 2.8 MPa. Aggregates are modelled with a static compressive strength of 150 MPa. Boundary and loading conditions are kept the same as the FE model described in the previous section. Fig. 10 shows the general mesoscale model setup.
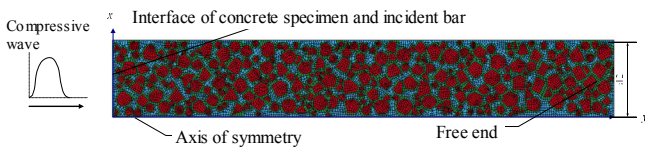

Figure 10: Mesoscale model configuration

Examination of the simulated stress and strain time histories (not shown) indicates a favourable comparison with the measured strain data during the experiment.

Fig. 11 presents the fracture patterns of the mesoscale model under the simulated experimental loading (30 MPa herein), along with those with increased load magnitudes of 40, 60 and 80 MPa, respectively. Note that these fracture patterns are shown in terms of the plastic strain, and it is capped (red colour) at 0.1 which roughly corresponds to about a 0.1mm crack width.

Under the experimental loading, fracture is dominated by a single macro crack, and this is consistent with the FE results shown in Fig. 6 and the experimental observation. Similar to the results from using the homogeneous model, more macro cracks tend to develop as the loading rate further increases. Moreover, the tensile damage tends to spread over an increasingly wider area as the loading rate increases, and this is demonstrated in the damage contours as shown in Fig. 12. As a result, the total energy dissipated over the entire damage region increases with the loading rate. The calculated amounts of fracture energy over the entire tensile damage region are listed in Table 3 in comparison with the results from the homogeneous model.
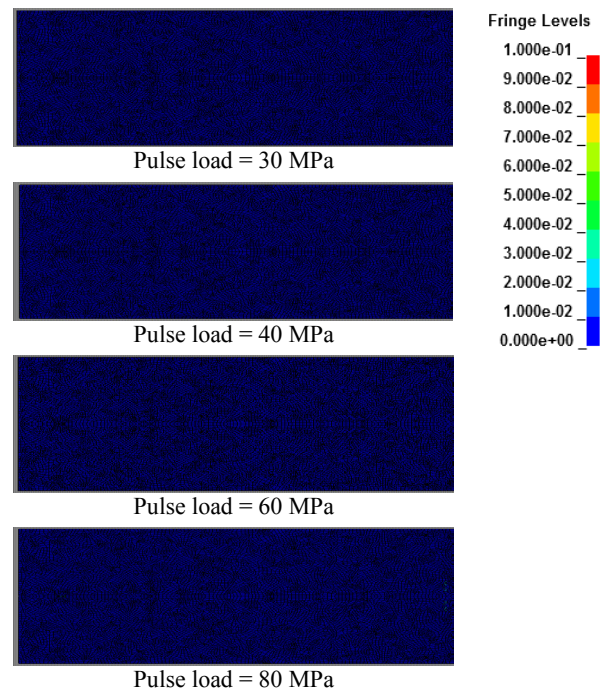

Figure 11: Macro crack patterns (represented by final plastic strain) of the mesoscale model under different loading & rates
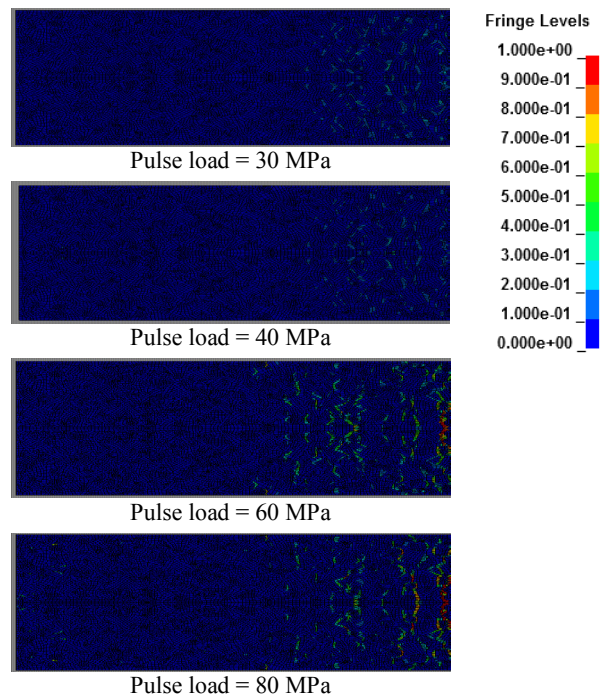

Figure 12: Distribution of tensile damage in the mesoscale model under different loading & rates

Comparing the damage contours shown in Fig. 12 with the homogeneous model in Fig. 6 & 9, it can be observed that with the presence

of the heterogeneity, the tensile damage exhibits a more distributed manner over a wider region. This is particularly true for the 60 MPa and 80 MPa loading scenarios. In fact the widths of the damage regions in these cases are much larger than a typical crack processing band of around 25 mm for the concrete under consideration. In such a situation, the fracture energy that is normally understood to associate with a distinctive crack "band" becomes less clearly defined and a unified approach taking into consideration of the nature of fracture spread under high strain rate tension would be required.

6   CONCLUDING REMARKS

A numerical model in the framework of continuum finite element method with a damage-plasticity material model incorporating mesh-objective softening is used for the simulation of fracture under high strain rate tension. A particular focus has been to explore the dynamic process of cracking and the development of the fracture zones.

Results from the preliminary simulations demonstrate that, for a tensile strain rate of order of 20 s^{-1}, the tension failure is still dominated by a single macro crack, which is in agreement with the respective spalling experiment. However, a significant tensile damage zone with a band width of around 30 mm has developed within the vicinity of the macro crack, both in the homogenous and the mesoscale models. As a result, the energy dissipation associated with such a fracture zone increases as compared to a lower loading rate condition, which transpires to an increase in the fracture energy. As the loading/strain rate further increases, a cluster of macro cracks can develop within an extended fracture zone, thus further increase the dynamic energy dissipation capacity. Comparison between the FE homogeneous model and the explicit mesoscale model indicates that with the inclusion of the aggregates the tensile damage tends to extend over an even wider range as the loading rate increases. This may be attributable to the regularisation effect of the stronger aggregates, and this phenomenon

warrants further investigation.

It should be noted that, with the propagating stress wave effect, the classical mesh-objective treatment of the softening behaviour in such an FE modelling framework could involve complications and this would affect quantitative interpretation of the dynamic fracture energy from the simulation results. Further work will look into better ways to handle the softening localisation in the wake of tensile damage spread due to the stress wave effect, with possible implementation of explicit crack-induced discontinuation. The more recent experiments [16] on notched specimen with direct recordings of the deformations of a single fracture zone will be used to evaluate the dynamic response and the features of the CSCM model.

REFERENCES

[1] Reinhardt, H.W. and Weerheijm, J., 1991. Tensile fracture of concrete at high loading rates taking account of inertia and crack velocity effects. *Int J Fracture*, **51**: 31-42.

[2] Donzé, F.V., Magnier, S.-A., Daudeville, L., Mariotti, C. and Davenne, L., 1999. Numerical study of compressive behavior of concrete at high strain rates. *J. Engineering Mechanics*. **125 (10)**: 1154-1163.

[3] Li, Q.M., Meng, H., 2003. About the dynamic strength enhancement of concrete-like materials in a split Hopkinson pressure bar test, *Int J Impact Eng*. **40:** 343-360.

[4] Lu, Y., Song, Z. and Tu, Z., 2009. Numerical simulation study of the strain rate effect on concrete in compression considering material heterogeneity. In: *Proc. DYMAT 2009*, September 7-11, 2009, Brussels.

[5] Hughes, M. L., Tedesco, J . W. and Ross, C. A., 1993. Numerical analysis of high strain rate slitting-tensile tests. *Computers & Structures*, **47(4/5)**: 653-671.

[6] Brara, A., Camborde, F., Klepaczko, J.R.

and Mariotti, C., 2001. Experimental and numerical study of concrete at high strain rates in tension. *Mech Mater* **33**: 33-45.

[7] Hentz, S., Donzé, F.V. and Daudeville, L., 2004. Discrete Element modeling of concrete submitted to dynamics loading at high strain rates. *Computers and Structures*, **82:** 2509-2524.

[8] Comite Euro-international du beton, Design of concrete structures. *CEB-FIP Model Code 1990*, Thomas Telford, 1993.

[9] Weerheijm, J., 1992. Concrete under impact tensile loading and lateral compression. *PhD Dessertation*, TU Delft.

[10] Schuler, H., Mayrhofer, C. and Thoma, K., 2006. Spall experiments for the measurement of the tensile strength and fracture energy of concrete at high strain rates, *Int J Impact Eng*. **32:** 1635–1650.

[11] Weerheijm, J., Van Doormaal, J.C.A.M., 2007. Tensile failure of concrete at high loading rates: New test data on strength and fracture energy from instrumented spalling tests, *Int J Impact Eng*. **34:** 609–626.

[12] Brara, A. and Klepaczko, J.R., 2007. Fracture energy of concrete at high loading rates in tension, *Int J Impact Eng*. **34:** 424–435.

[13] Klepaczko, J.R. and Brara, A., 2001. An experimental method for dynamic tensile testing of concrete by spalling, *Int J Impact Eng*. **25:** 387–409.

[14] Murray, Y. D., 2007. Users Manual for LS-DYNA Concrete Material Model 159. Springfield, VA, US Department of Transportation.

[15] Tu, Z. and Lu, Y., 2011. Mesoscale modelling of concrete for static and dynamic response analysis Part 1: model development and implementation. *Structural Engineering & Mechanics*. **37**: 197–213.

[16] Vegt, I., Weerheijm, J. and Breugel, K. van (2009) The rate dependency of concrete under tensile impact loading. Fracture energy and fracture characteristics. Conference Proceedings 13th ISIEMS.

[17] Ozbolt, J. Weerheijm, J. and Sharma, A. (2013) Dynamic tensile resistance of concrete – Split Hopkinson Bar test. FramCos8, Toledo, Spain.